Bull. Chem. Soc. Ethiop. **2015**, 29(1), 137-148.
Printed in Ethiopia
DOI: http://dx.doi.org/10.4314/bcse.v29i1.13
ISSN 1011-3924

SYNTHESIS, CHARACTERIZATION AND DENSITY FUNCTIONAL THEORY STUDY OF LOW COST HYDRAZONE SENSITIZERS

Abdullah G. Al-Sehemi[1,2,3*], Ahmad Irfan[1*], Abdullah M. Asiri[4,5], Yousry Ahmed Ammar[1]

[1]Department of Chemistry, Faculty of Science, King Khalid University, Abha 61413, P.O. Box 9004, Saudi Arabia
[2]Unit of Science and Technology, Faculty of Science, King Khalid University, Abha 61413, P.O. Box 9004, Saudi Arabia
[3]Research Center for Advanced Materials Science, King Khalid University, Abha 61413, P.O. Box 9004, Saudi Arabia
[4]Chemistry Department, Faculty of Science, King Abdulaziz University, P.O. Box 80203, Jeddah 21589, Saudi Arabia
[5]The Center of Excellence for Advance Materials Research, King Abdulaziz University, P.O. Box 80203, Jeddah 21589, Saudi Arabia

(Received December 22, 2013; revised September 26, 2014)

ABSTRACT. The 2-{4-[2-benzylidenehydrazino]phenyl}ethylene-1,1,2-tricarbonitrile (System 1), 2-{4-[2-(1-naphthylmethylene)hydrazino]phenyl}ethylene-1,1,2-tricarbonitrile (System 2) and 2-{4-[2-(9-anthrylmethylene)-hydrazino]phenyl}ethylene-1,1,2-tricarbonitrile (System 3) were synthesized by direct tricyanovinylation of hydrazones. The bathochromic shift in absorption spectra has been observed by increasing the solvent polarity. The FTIR spectra of these new dyes exhibited three important absorption bands. The first band centered near 3260 cm^{-1} in System 1 while 3208 cm^{-1} and 3211 cm^{-1} in System 2 and System 3 for the νNH absorption, respectively. The second band is a sharp absorption band in the region of 2212-2209 cm^{-1}, which was attributed to the cyano group absorption. The third is an absorption band in the region of 1611-1603 cm^{-1} ascribed for the C=N. Density functional theory (DFT) calculation of relative energies, relative enthalpies and free energies shows that E isomers are the most stable except System 3 in which the most stable is Z isomers. The conformational energy profile shows two maxima near (-90 and 90°) while three local minima observed at (-180, 0 and 180) for N1-N2-C1-C2 torsional angle. The highest occupied molecular orbitals (HOMOs) are localized on the whole molecules while lowest unoccupied molecular orbitals (LUMOs) are distributed on the tricarbonitrile.

KEY WORDS: Dye-sensitized solar cells, HOMO, LUMO, Absorption, FTIR spectra

INTRODUCTION

The basic design of today's high performance dye sensitized solar cells (DSSC) was developed in the early 1990's by Grätzel *et al.* [1]. They have great potential applications in the fields of electronics, optics, catalysis and energy storage/conversion [1]. The DSSC have been extensively investigated due to their simple structure, low cost and environmental friendly [2-4]. It is assumed that the world energy demand will increase by about 70% between 2000 and 2030. Fossil fuels are facing rapid resource depletion which is supplying 80% of all energy consumed worldwide. The resource reserves of fossil fuels throughout the whole world in 2002 were projected to last 40 years for oil, 60 years for natural gas and 200 years for coal. Because of a growing demand for energy, there is an urgent need for environmentally sustainable energy technologies. Among all the renewable energy technologies, such as wind turbines, hydropower, wave and tidal power, solar cells, solar thermal, biomass-derived liquid fuels and biomass-fired electricity generation, photovoltaic technology utilizing solar energy is considered as the most promising one [5]. An ideal light harvesting system absorbs light efficiently in a relatively broad region covering most of the sunlight spectrum. In order to achieve this, the integration of multiple excellent chromophores is necessary, and the energy transfer within the system should

*Corresponding author. E-mail: irfaahmad@gmail.com

be efficient. The development of highly efficient light-harvesting systems remains a challenging task. There is need in improvement like the choice of the chromophores, linker types, connection sites, and synthesis strategy etc.

Dye is an important part in DSSCs, which absorbs the light and then generates electric current. Up till now there are two kinds of dye sensitizers, metal-organic complexes and metal-free organic dyes. In metal-organic complexes, especially the noble metal ruthenium polypyridyl complexes, including N3 and black dye that were presented by Gratzel *et al.* [1] have given best performance among the dye sensitizers with on the whole energy change efficiency greater than 10%. On the other hand, metal-free organic dyes as sensitizers for DSSC, together with cyanines, hemicyanines, triphenylmethanes, perylenes, coumarins, squaraines, indoline, and azulene-based dyes have also been formed due to their high molar absorption coefficient, relatively simple synthesis procedure, various structures and lower cost [6].

In contrast to the numerous experimental studies of dye sensitizers, the theoretical investigations are comparatively inadequate. Only several groups focused on the electronic structures, absorption properties of dye sensitizers, Ru-complexes and organic dyes coupled TiO_2 nanocrystalline as well as the electron transfer dynamics of the interface between dyes and nanocrystalline. Until now, it is a severe challenge for both experiment and theory to make clear the fundamental properties of the ultrafast electron injection and come up to the satisfied efficiency of DSSC. Further developments in dye design will play a vital part in the continuing optimization of DSSC and it depends on the quantitative knowledge of dye sensitizer. So the theoretical investigations of the physical properties of dye sensitizers are very important in order to disclose the relationship among the performance, structures and the properties, it is also supportive to design and production of novel dye sensitizers with higher performance [7, 8].

The conjugated π-system contains asymmetrically positioned electron-donor and electron-acceptor substituents have been the most widely studied [9]. The charge transfer between the functional groups imparts a high degree of polarity to push-pull systems. The electronic and structural properties of donor-acceptor substituted π-conjugated organic compounds are of considerable interest because of their applicability to electrooptic devices and data storage [10, 11]. A wide variety of structural modifications on the donor-acceptor and conjugated moieties have been carried out [12, 13]. It is well known that by increasing donor, acceptor strengths and with increasing length of conjugation charge transfer properties can be enhanced [14]. Many donor acceptors conjugated organic molecules reported in the literature fall into the following categories: substituted benzene, biphenyls, stilbenes, azobenzenes, ferrocenyl and Schiff bases [15-17]. In all these classes, benzene rings with or without the π-bridges have been employed as the conjugated moieties to connect donor. We have synthesized different derivatives of hydrazones. We report on the synthesis of the novel push-pull system based on hydrazones. By substituting benzyl, naphthyl and anthryl groups as donor, the effect on electronic, spectroscopic especially absorption and FTIR has been investigated. We have shed light on the electronic and optical properties by density functional theory (DFT) as well. We have also discussed the structure-property relationship.

The article describes the synthesis of the targeted materials, the framework of the Density Functional Theory (DFT) and Time Dependent Density Functional Theory (TDDFT), the geometries, electro-optical properties, thermo-dynamical properties, FTIR spectra and conformational analysis.

EXPERIMENTAL

The hydrazone derivatives were prepared through direct condensation between the corresponding aromatic aldehydes and phenyl hydrazine Scheme 1. Equimolar quantities of phenylhydrazine and the aldehydes were boiled in ethanol for half an hour. The precipitated hydrazones were filtered, washed and dried. The pure hydrazones were obtained after recrystallization from ethanol.

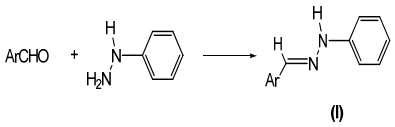

(I)

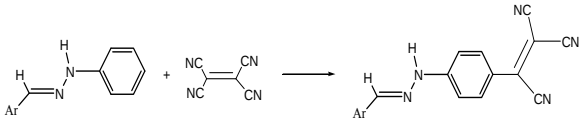

No	1a	1b	1c
Ar			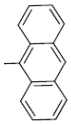

No	System 1	System 2	System 3
Ar			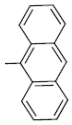

Scheme I Scheme II

Scheme 1. Schematic diagram of investigated Systems.

Benzaldehyde phenylhydrazone [($C_{13}H_{12}N_2$ (196.25)]. M.p. 150-152 ^oC, yield 93%, R_f 0.61 (9:1), ^1H NMR ($CDCl_3$): d 6.82 (t, 1H), 7.13 (d, 2H), 7.27 (d, 2H), 7.40-7.67 (m, 5H), 8.17 (s, 1H).

1-Naphthaldehyde phenylhydrazone [$C_{17}H_{14}N_2$(246.31)]. M.p. 72-74 ^oC, yield 91%, R_f 0.74 (8:2), ^1H NMR ($CDCl_3$): d 6.89 (bs, 1H, NH), 7.16-7.82 (m, 7H, naph-H), 7.84 (s, 5H, Ph-H), 8.0 (d, 1H, CH).

9-Anthraldehyde phenylhydrazone [$C_{21}H_{16}N_2$(296.37)]. M.p. 199-200, yield 21%, R_f 0.35 (9:1), ^1H NMR ($CDCl_3$): d 7.31-7.63 (m, 14H, Ph-H), 9.13 (s, 1H, CH=N).

The new chromospheres were prepared by direct tricyanovinylation of hydrazones and this was achieved by mixing together the appropriate hydrazones and tetracyanoethylene (TCNE), as shown in Scheme 2. All the prepared chromospheres were obtained as dark violet solids. A solution of the requisite hydrazone 1 (0.01 mol) and TCNE in DMF (20 mL) was stirred at 60-90 ^oC for 5-7 h. The solvent was removed and the residual solid was collected and recrystallized from toluene/chloroform mixture.

System 1: 2-{4-[2-Benzylidenehydrazino]phenyl}ethylene-1,1,2-tricarbonitrile [$C_{18}H_{11}N_5$ (297.31)]. M.p. 285-288 ^oC, yield 76%, UV-Vis (acetone): λ_{max} (nm) 525, 333; FTIR (cm^{-1}): 3262 (sec. NH), 2212 (CN), 1609 (C=N), 1337 (C-N); ^1H NMR (DMSO-d_6): 7.42-8.01 (m, 9H,Ar-H), 8.14 (s, 1H, CH=N), 11.84 (s, 1H, NH; cancelled with D_2O). ^{13}C NMR (DMSO-d_6): 79.56, 144.48 (C=C), 3x114.8 (3CN), 112.95, 113.9, 119.4, 126.6, 2x128.8, 2x129.9, 132.7, 134.2, 137.3, 151.19 (12C-Ar), 162.29 (CH=N).

System 2: 2-{4-[2-(1-Naphthylmethylene)hydrazino]phenyl}ethylene-1,1,2-tricarbonitrile [$C_{22}H_{13}N_5$(347.37)]. M.p. 268-270 ^oC, yield 87%; UV-Vis (acetone): λ_{max} (nm) 529, 353; FTIR $\nu(cm^{-1})$: 3208 (sec. NH), 2212 (CN), 1611 (C=N), 1341 (C-N); ^1H NMR ($CDCl_3$): δ 7.37-8.05 (m, 11H, Ar-H), 8.76(s, 1H, CH=N), 11.95(s, 1H, NH); ^{13}C NMR (DMSO-d_6): 78.15, 144.48

(C=C), 3x114.84 (3CN), 113.94, 2x119.52, 123.96, 125.61, 2x126.30, 127.52, 127.68, 128.88, 129.41, 129.62, 130.44, 132.84, 133.57, 137.32(16C-Ar), 162.27 (CH=N).

System 3: 2-{4-[2-(9-Anthrylmethylene)hydrazino]phenyl}ethylene-1,1,2-tricarbonitrile [$C_{26}H_{15}N_5$ (397.43)]. M.p. 247-248 ^{o}C, yield 74%; UV-Vis (acetone): λ_{max} (nm) 540, 407; FTIR ν(cm^{-1}): 3211 (sec. NH), 2209 (CN), 1603 (C=N), 1334 (C-N); ^{1}H NMR (DMSO-d_6): 6.80-8.20 (m, 13H, Ar-H), 8.30(s, 1H, CH=N), 10.80 (s, 1H, NH). ^{13}C NMR (DMSO-d_6): 79.0, 143.40, (C=C), 3x112.49 (3CN), 111.86, 118.93, 120.22, 124.18, 124.64, 124.90, 125.31, 125.48, 125.75, 126.87, 127.38, 128.17, 128.64, 128.96, 129.23, 129.70, 130.90, 132.31, 132.87, 135.03 (20C-Ar), 162.50 (C=N).

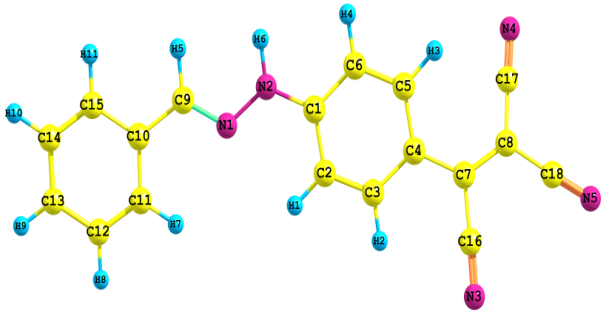

System 1-E

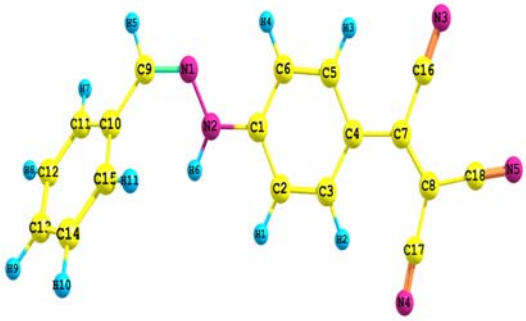

System 1-Z

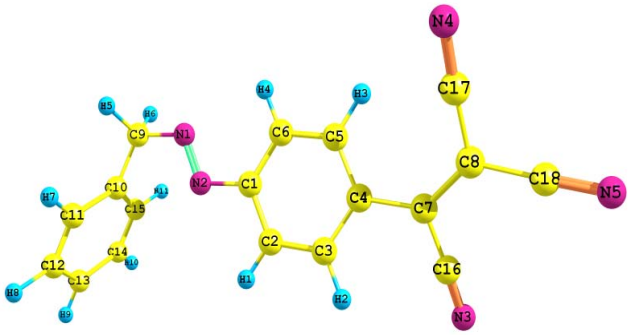

System 1-azo

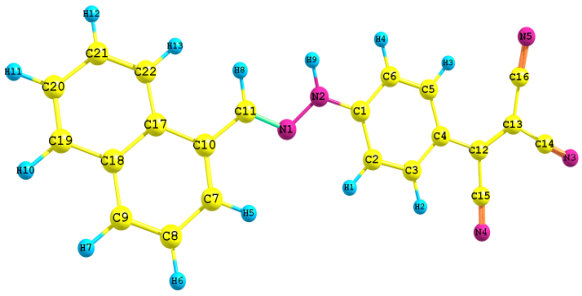

System 2-E

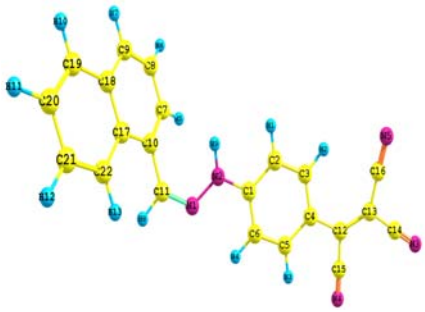

System 2-Z

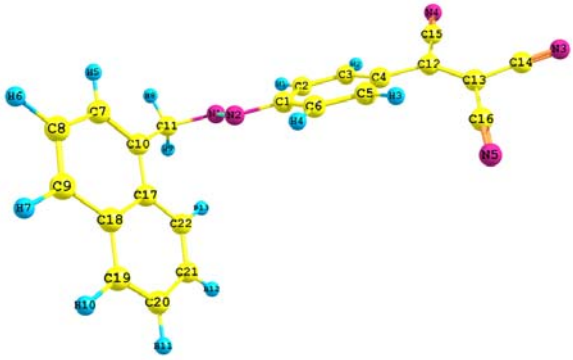

System 2-azo

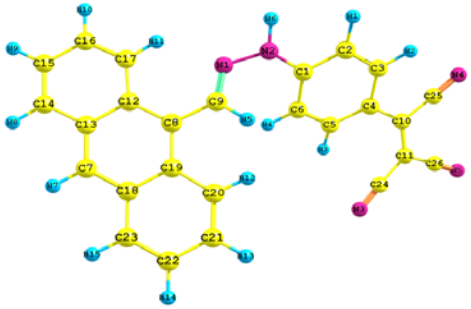

System 3-E

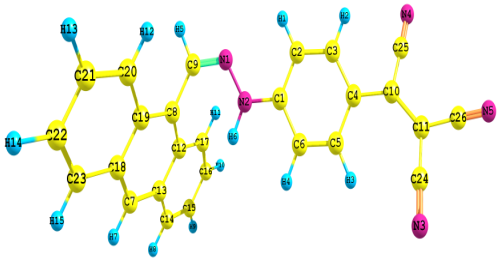

System 3-Z

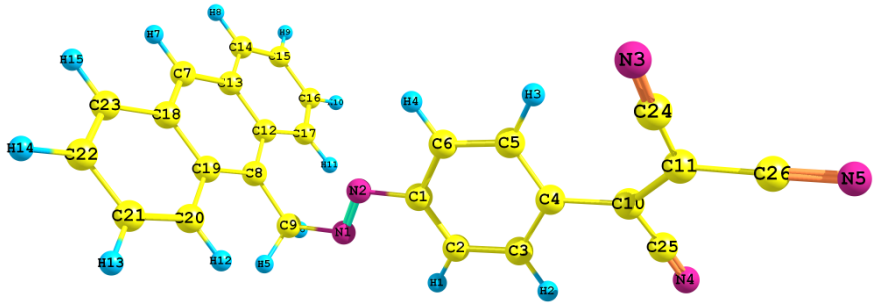

System 3-azo

Figure S1. Three possible classes of isomeric molecules for E, Z and azo isomerism.

Computational methods

Recently, it has been shown that Density Functional Theory (DFT) calculations with B3LYP/6-31G(d) level of theory is approach to reproduce the experimental data of the hydrazones [18]. The molecular structures of dye compounds have been optimized using DFT calculations with B3LYP/6-31G(d) level of theory [19-22]. The Time Dependent (TD-DFT) has been applied to compute the absorption spectra at the B3LYP/6-31G(d) level of theory which has been proved to be accurate and reliable method [23, 24]. Thermodynamic parameters i.e., relative energies (ΔE_0), enthalpies (ΔH) and free energies (ΔG) (kcal/mol) for E, Z and azo isomers (See Figure S1) of studied Systems have been computed at B3LYP/6-31G(d) level of theory. All of the DFT calculations were done using Gaussian-03 program package [25]. These isomers arise by rotating around torsion angles N1-N2-C1-C2 for investigated dyes. Then by fully optimization of the resulting structures the stable conformers were obtained.

RESULTS AND DISCUSSION

Geometries

The fully optimized structures of studied isomers are shown in Figure S1. The computed geometrical parameters of all the conformers have been given in Table 1. The C-C, C-N and N-N bond lengths of *E* and *Z* isomer of all the investigated systems are almost same while the C_9-C_{10} in *Z* isomer of System 2 and System 3 stretched compared to System 1. Similarly, the C_9-C_{10} in azo isomer of System 2 and System 3 lengthened compared to System 1. By comparing the bond lengths of the *E*, *Z* and azo isomer of System 1, we have observed that C_9-C_{10} of *Z* isomer lengthened 0.017 Å while azo isomer stretched 0.040 Å compared to *E* isomer. The C_9-N_1 and N_2-C_1 of azo isomer elongated almost 0.191 and 0.059 Å than *E* and *Z* isomers while N_1-N_2 shortened 0.105 Å. In System2 the C_9-C_{10} of *Z* isomer lengthened 0.019 Å and azo isomer stretched 0.048 Å compared to *E* isomer. The C_9-N_1 and N_2-C_1 of azo isomer elongated almost 0.190 and 0.059 Å than *E* and *Z* isomers while N_1-N_2 shortened 0.105 Å. The change in the bond lengths between *E*, *Z* and azo isomers in System 3 is nearly alike as System 1 and System 2. The torsion of *E* isomers in System 1 and System 2 is smaller than *Z* and azo isomers.

Table 1. Optimized geometrical parameters of investigated systems at B3LYP/6-31G* level of theory.

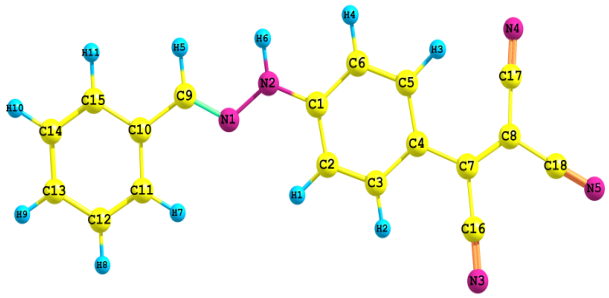

	Bond lengths (Å)						
System	C9-C10	C9-N1	N1-N2	N2-C1	C1-C2	C1-C6	C4-C7
System 1-*E*	1.460	1.289	1.353	1.373	1.410	1.412	1.457
System 1-*Z*	1.477	1.290	1.357	1.376	1.409	1.411	1.457
System 1-azo	1.500	1.481	1.248	1.432	1.398	1.404	1.471
System 2-*E*	1.462	1.290	1.352	1.373	1.410	1.412	1.456
System 2-*Z*	1.481	1.290	1.356	1.375	1.411	1.409	1.457
System 2-azo	1.510	1.480	1.248	1.431	1.403	1.399	1.471
System 3-*E*	1.461	1.294	1.359	1.379	1.414	1.416	1.455
System 3-*Z*	1.489	1.289	1.355	1.374	1.411	1.410	1.457
System 3-azo	1.511	1.480	1.249	1.431	1.399	1.403	1.471
Dihedral angles (degrees)							
	C10-C9-N1-N2		C9-N1-N2-C1		N1-N2-C1-C2		
System 1-*E*	-180.0		-179.9		-0.117		
System 1-*Z*	2.002		177.1		-173.1		
System 1-azo	-1.003		-180.0		178.5		
System 2-*E*	-178.6		-179.2		0.415		
System 2-*Z*	3.174		176.6		-175.3		
System 2-azo	-4.348		-178.8		6.461		
System 3-*E*	179.8		53.8		175.3		
System 3-*Z*	-0.877		-178.8		-2.956		
System 3-azo	0.337		179.9		-0.946		

Electronic and optical properties

Figure 1 illustrates the distribution pattern of the highest occupied molecular orbitals (HOMO) and lowest unoccupied molecular orbitals (LUMO). As can be seen clearly, HOMO is concentrated on the whole molecules and lone pair of electron on the N atoms. The LUMO is of antibonding character with π* character distributed on the tricarbonitrile except System 1 in which it is delocalized on whole of the molecule. It is might be due to donor group strength; as in System 2 and System 3 naphthyl and anthryl groups are more donor than benzyl of System 1 due to which in System 2 and System 3 LUMO shifted towards tricarbonitrile. The HOMO-LUMO energy gap of these dyes was calculated at the B3LYP/6-31G(d) level of theory, see Table 2. The orbital energy level analysis at the B3LYP/6-31G(d) level of theory show HOMO energy (E_{HOMO}), LUMO energy (E_{LUMO}) and HOMO–LUMO energy gap (E_{gap}) has been used as an indicator of kinetic stability of the molecule. A large HOMO–LUMO gap implies a high kinetic stability and low chemical reactivity, because it is energetically unfavorable to add electrons to a high-lying LUMO or to extract electrons from a low-lying HOMO. The trend of E_{gap} is System 1 > System 2 > System 3. Generally it is said that low E_{gap} leads to red shift which is in good agreement with experimental absorption tendency System 3 > System 2 > System 1.

Efficient DSSC sensitizers have narrow band gap with LUMO lying just above the conduction band of TiO_2 and HOMO below the redox couple. As a model for nanocrystallinity the HOMO and LUMO energies of bare cluster $(TiO_2)_{38}$ are -7.23 and -4.1 eV, respectively, resulting in a E_{gap} of 3.13 eV [26]. Generally energy gap more than 0.2 eV between the LUMO of the dye and the conduction band of the TiO_2 is necessary for effective electron injection [27]. The LUMO energies of studied dyes are above the conduction band of TiO_2. The HOMO of the redox couple (I^-/I_3^-) is -4.8 eV [28]. It can be found that HOMOs of the dyes are below the redox couple. The smaller HOMO-LUMO energy gaps revealed that these dyes would be efficient for DSSC.

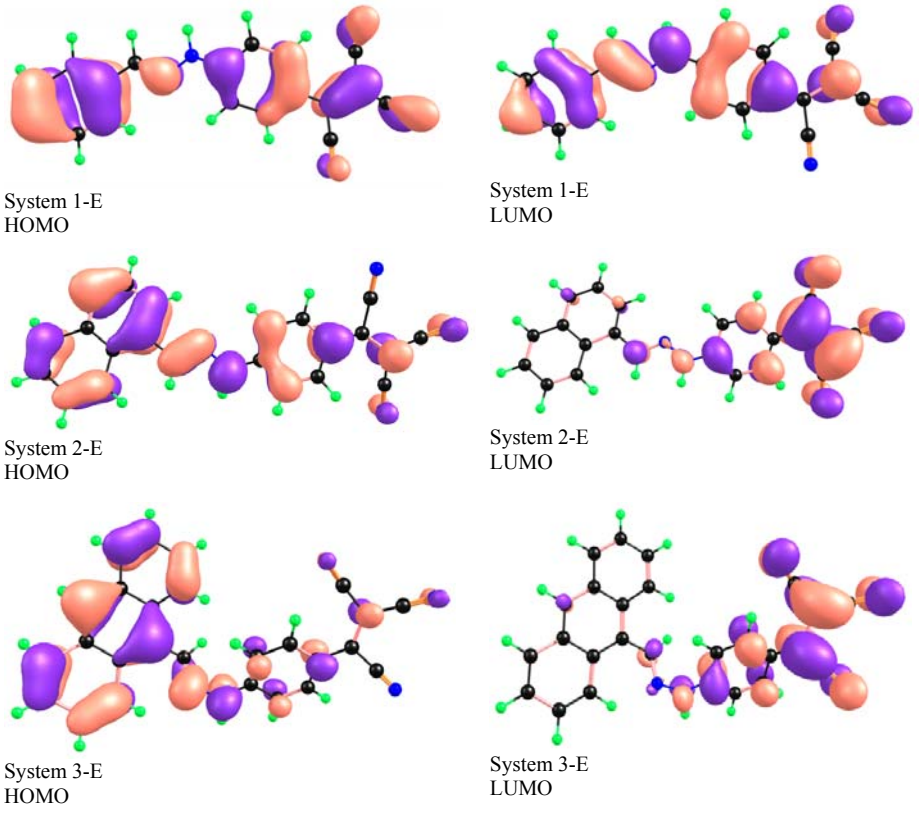

Figure 1. The distribution pattern of HOMOs and LUMOs of the System 1-3.

Table 2. HOMO energy (E_{HOMO}), LUMO energy (E_{LUMO}) and HOMO–LUMO energy gap (E_{gap}) calculated (eV) at B3LYP/6-31G* level of theory.

Dyes	E_{HOMO}	E_{LUMO}	E_{gap}
System 1	-6.02	-3.31	2.71
System 2	-5.84	-3.30	2.54
System 3	-5.60	-3.29	2.31

The electronic absorption spectra of the new chromospheres are characterized by an intense, low-energy band that is dependent on the nature of the substituent. System1 showed absorption band at 523 nm in chloroform. A substitution of phenyl group by 1-naphthyl, e.g. System 2 showed a bathochromic shift of 12 nm compared with the System 1. System 3, in addition to substitution of the phenyl group with 9-anthryl group caused a bathochromic shift of 20 nm compared to System 1, see Table 3.

Table 3. The effects of solvents on the absorption maxima (nm) of investigated dyes.

Dyes	λ_{max}								
	a	b	c	d	e	f	g	ε_{max}	$\Delta\lambda$
System 1	525 333	522	550 316	523 317	516 315	507	558 318	45662 10564	51
System 2	529 353	528 354	528 350	535 354	522 350	517 354	570 359	21145 5568	53
System 3	540 407	535 405	527 407	543 411	524 405	519 407	593 411	21062 9406	74

a = CH_3COCH_3, b = CH_3CN, c = CH_3COOH, d = $CHCl_3$, e = $(C_2H_5)_2O$, f = $PhCH_3$, g = $(CH_3)_2NCHO$.

The dyes were measured in various solvents having different polarity. In non-polar solvents for instance in ether System 3 showed the most solvatochromic shift with absorption maxima at 524 nm while in the DMF the maxima is at 593 nm. The solvatochromic effect can be estimated from the difference between the absorption maxima in polar and non-polar solvents, e.g. $\Delta\lambda$. The solvent's effects can be rationalized on the basis of the dipole formed by charge migration from the nitrogen to the acceptor tricyanovinyl (Scheme 2).

FTIR spectra

The FTIR spectra of hydrazones exhibited two important absorption bands; the first band centered near 3300 cm^{-1} for the νNH absorption. The second band is a sharp absorption band in the region of 1598 cm^{-1} ascribed for the CH=N absorption.

The FTIR spectra of these new dyes exhibited three important absorption bands; the first band centered near 3260 cm^{-1} in System 1 while 3208 cm^{-1} and 3211 cm^{-1} in System 2 and System 3 for the νNH absorption. The second band is a sharp absorption band in the region of 2212-2209 cm^{-1}, which was attributed to the cyano group absorption. The third is an absorption band in the region of 1611-1603 cm^{-1} ascribed for the C=N absorption. The tricyanovinylation undoubtedly takes place at a position para to the hydrazine group as evidenced from the ^1H NMR signals for the doublet two hydrogens. The azomethine hydrogen of the synthesized dyes was located in the region of 8.1-9.13 ppm.

Thermodynamic stabilities

Thermodynamic parameters and energy barrier for the dyes have been computed at B3LYP/6-31G(d) level of theory, see Table 4. The relative energy, ΔE_0, is defined as a difference between its zero-point corrected total energy and that of the most stable one *E*. Relative enthalpies and free energies at 298 ^oK are also defined as the difference between the enthalpy or free energy (in kcal/mol) of a given *E/Z* or *azo* isomers and that of *E* form. As shown in Table 2, the order of relative stability of those isomers is the same when considering relative energy or relative free energy. DFT calculation shows that *E* isomers are the most stable except System3 in which the most stable is *Z* isomers. We have observed that dipole moment of *Z* isomer is highest while azo isomer is lowest. The trend in different isomers is *Z* > *E* > azo.

Table 4. Thermodynamic parameters (kcal/mol) for *E*, *Z* and azo isomers of studied Systems at B3LYP/6-31G(d) level of theory.

System	ΔE_0	ΔH	ΔG	ΔE	Dipole moment
System 1 *E*	0.00	0.00	0.00	0.00	12.0721
System 1 *Z*	4.41	3.76	6.02	4.10	12.7074
System 1 azo	16.4	16.5	15.8	17.1	7.1234
System 2 *E*	0.00	0.00	0.00	0.00	12.502
System 2 *Z*	2.54	2.37	2.90	2.12	13.0342
System 2 azo	14.82	14.76	14.86	15.26	7.0346
System 3 *E*	7.82	7.98	7.54	7.78	10.9088
System 3 *Z*	0.00	0.00	0.00	0.00	12.5737
System 3 azo	13.8	13.9	12.8	14.5	7.1099

Conformation analysis

For modeling and scanning calculation the initial guess for the stable isomers E was first obtained from the optimization using B3LYP/6-31G(d) and transformed into the Z-matrix format with Babel program [29]. The starting geometry of E-isomers was obtained by driving procedure in HyperChem [30]. To predict the rotation barriers around the N1-N2-C1-C2 torsional angle scanning calculations were done. To identify low energy conformations, the potential energy surface shape has been examined at the B3LYP/6-31G(d) level of theory. The potential energy surfaces of dihedral angle (N1-N2-C1-C2) from $+180^o$ to -180^o in 5^o or 10^o steps were performed (Figure 2). The conformational energy profile shows two maxima near (-90 and 90^o). The aromatic rings are nearly perpendicular at these values of selected torsion angle. The energy barriers may be due to the steric interactions between the π-electrons of the two aromatic rings. It is clear from Figure 2, there are three local minima observed at (-180, 0 and 180) for N1- N1-N2-C1-C2 torsional angle and these are most stable conformers for this torsion angle. The DFT optimized geometry of these dyes is coplanar at these values of selected torsion angle.

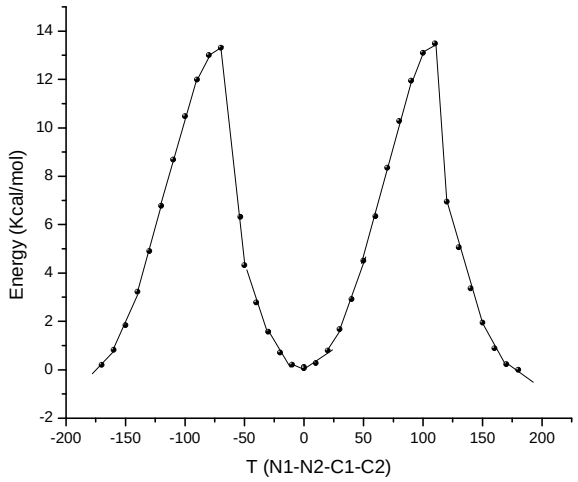

Figure 2. Molecular energy profile using DFT against the selected torsional degree of freedom of System 2.

CONCLUSIONS

The DFT calculations of thermodynamic parameters revealed that the most stable isomers are *E* with the exception of System 3 (*Z* isomer). The HOMOs are localized on entire molecule while LUMOs distributed on the tricarbonitrile except System 1 (in which delocalization was observed on entire molecule). By increasing the solvent polarity red shift in the absorption wavelengths have been observed. The FTIR spectra of the investigated dyes showed three significant absorption bands. Clear intra-molecular charge transfer has been observed in System 2 and System 3. The LUMO energies of studied dyes are above the conduction band of TiO_2 while the HOMOs of the dyes are below the redox couple. The smaller HOMO-LUMO energy gaps revealed that these dyes would be efficient for DSSC.

ACKNOWLEDGEMENTS

The present work has been carried out under project No. 08-NAN155-7 funded by KAUST (King Abdulaziz City for Science and Technology) through the Long Term Comprehensive National Plan for Science, Technology and Innovation program.

REFERENCES

1. O'Reagan, B.; Grätzel, M. *Nature* **1991**, 353, 737.
2. Imahori, H.; Umeyama, T.; Ito, S. *Acc. Chem. Res*. **2009**, 42, 1809.
3. Kalyanasundaram, K.; Gratzel, M. *Coord. Chem. Rev*. **1998**, 177, 347.
4. Hagfeldt, A.; Gratzel, M. *Acc. Chem. Res*. **2000**, 33, 269.
5. Gratzel, M. *Nature* **2001**, 414, 338.
6. Jia, C.; Wan, Z.; Zhang, J.; Li, Z.; Yao, X.; Shi, Y. *Spectrochim. Acta Part A: Mol. Biomol. Spectr*. **2012**, 86, 387.
7. Preat, J.; Jacquemin, D.; Perpète, E.A. *Environ. Sci. Technol*. **2010**, 44, 5666.
8. Preat, J.; Hagfeldt, A.; Perpète, E.A. *Energy Environ. Sci*. **2011**, 4, 4537.
9. Bloembergen, N. *Nonlinear Optics*, Benjamin: New York; **1965**.
10. Asiri, M.; Ismail, M.I.; Al-Amry, K.A.; Fatani, N.A. *Dyes and Pigments* **2005**, 67, 111.
11. Marder, S.R.; Sohn, J.E.; Stucky, G.D. *Materials for Nonlinear Optics: Chemical Perspectives* in *ACS Symposium Series*, ACS: Washington, DC; **1991**; p 455.
12. Marder, S.; Gorman, C.B.; Tiemann, B.G.; Cheng, L.T. *J. Am. Chem. Soc*. **1993**, 115, 3006.
13. Wang, Y.K.; Shu, C.-F.; Breitung, E.M.; McMahon, J. *J. Mater. Chem*. **1999**, 9, 1449.
14. Peng, Q.; Park, K.; Lin, T.; Durstock, M.; Dai, L. *J. Phys. Chem*. **2008**, B 112, 2801.
15. Singer, K.D.; Sohn, J.E.; King, L.A.; Gordon, H.M.; Katz, H.E.; Dirk, C.W. *J. Opt. Soc. Am*. **1989**, B6, 1339.
16. Shu, C.-F.; Wang, Y.-K. *J. Mater. Chem*. **1998**, 8, 833.
17. Asiri, A.M. *Appl. Organomet. Chem*. **2001**, 15, 907.
18. (a) Al-Sehemi, A.G.; Irfan, A.; Asiri, A.M. *Theor. Chem. Acc*. **2012**, 131, 1199. (b) Al-Sehemi, A.G.; Irfan, A.; Asiri, A.M.; Ammar, Y.A. *Spectrochimica Acta Part A* **2012**, 91, 239. (c) Al-Sehemi, A.G.; Irfan, A.; Asiri, A.M.; Ammar, Y.A. *J. Mol. Struc*. **2012**, 1019, 130. (d) Irfan, A.; Al-Sehemi, A.G.; Al-Assiri, M.S. *J. Fluorine Chem*. **2014**, 157, 52. (e) Irfan, A. *Comput. Mater. Sci.* **2014**, 81, 488. (f) Irfan, A. *Mater. Chem. Phys.* **2013**, 142, 238. (g) Irfan, A.; Al-Sehemi, A.G.; Al-Assiri, M.S. *J. Mol. Graphics Model.* **2013**, 44, 168. (h) Irfan, A. *Optik* **2014**, 125, 4825. (i) Irfan, A.; Al-Sehemi, A.G.; Al-Assiri, M.S. *Comput. Theor. Chem.* **2014**, 1031, 76. (j) Irfan, A. *J. Theor. Comput. Chem*. **2014**, 13, 1450013. (k) Irfan, A.; Al-Sehemi, A.G.; Muhammad, S. *Synthetic Metals* **2014**. 190, 27. (l) Irfan, A.

Bull. Chem. Soc. Ethiop. **2014**, 28, 101. (m) Sehemi, A.G.; Al-Amri, R.S.A.A.; Irfan, A. *Bull. Chem. Soc. Ethiop*. **2014**, 28, 111.
19. (a) Becke, A.D. *J. Chem. Phys*. **1993**, 98, 5648. (b) Lee, C.; Yang, W.; Parr, R.G. *Phys. Rev*. **1988**, B37, 785.
20. Stephens, P.J.; Devlin, F.J.; Chabalowski, C.F.; Frisch, M.J. *J. Phys. Chem*. **1994**, 98, 11623.
21. Lynch, B.J.; Fast, P.L.; Harris, M.; Truhlar, D.G. *J. Phys. Chem*. **2000**, A 104, 4811.
22. Perdew, J.P.; Chevary, J.A.; Vosko, S.H.; Jackson, K.A.; Pederson, M.R.; Singh, D.J.; Fiolhais, C. *Phys. Rev*. **1992**, B46, 6671.
23. Walsh, P.J.; Gordon, K.C.; Officer, D.L.; Campbell, W.M. *J. Mol. Struc-Thechem*. **2006**, 759, 17.
24. Cleland, D.M.; Gordon, K.C.; Officer, D.L.; Wagner, P.; Walsh, P.J. *Spectrochim. Acta Part A* **2009**, 74, 931.
25. Frisch, M.J.; Trucks, G.W.; Schlegel, H.B.; Scuseria, G.E.; Robb, M.A.; Cheeseman, J.R.; Scalmani, G.; Barone, V.; Mennucci, B.; Petersson, G.A.; Nakatsuji, H.; Caricato, M.; Li, X.; Hratchian, H.P.; Izmaylov, A.F.; Bloino, J.; Zheng, G.; Sonnenberg, J.L.; Hada, M.; Ehara, M.; Toyota, K.; Fukuda, R.; Hasegawa, J.; Ishida, M.; Nakajima, T.; Honda, Y.; Kitao, O.; Nakai, H.; Vreven, T.; Montgomery, J.A., Jr.; Peralta, J.E.; Ogliaro, F.; Bearpark, M.; Heyd, J.J.; Brothers, E.; Kudin, K.N.; Staroverov, V.N.; Kobayashi, R.; Normand, J.; Raghavachari, K.; Rendell, A.; Burant, J.C.; Iyengar, S.S.; Tomasi, J.; Cossi, M.; Rega, N.; Millam, N.J.; Klene, M.; Knox, J.E.; Cross, J.B.; Bakken, V.; Adamo, C.; Jaramillo, J.; Gomperts, R.; Stratmann, R.E.; Yazyev, O.; Austin, A.J.; Cammi, R.; Pomelli, C.; Ochterski, J.W.; Martin, R.L.; Morokuma, K.; Zakrzewski, V.G.; Voth, G.A.; Salvador, P.; Dannenberg, J.J.; Dapprich, S.; Daniels, A.D.; Farkas, Ö.; Foresman, J.B.; Ortiz, J.V.; Cioslowski, J.; Fox, D.J. *Gaussian 09, Revision A.1*, Gaussian, Inc.: Wallingford, CT; **2009**.
26. Balanay, M.P.; Kim, D.H. *Phys. Chem. Chem. Phys*. **2008**, 10, 5121.
27. Angelis, F.D.; Fntacci, S.; Selloni, A. *Nanotechnology* **2008**, 19, 424002.
28. Ito, S.; Zakeeruddin, S.M.; Humphry-Baker, R.; Liska, P.; Charvet, R.; Comte, P.; Nazeeruddin, M.K.; Péchy, P.; Takata, M.; Miura, H.; Uchida, S.; Grätzel, M. *Adv. Mater*. **2006**, 18, 1202.
29. Walters, P.; Stahl M.B, *Version 1.1*, Department of Chemistry, University of Arizona: Tucson, Arizona; **1994**.
30. Hyper Chem 7.5, *Molecular Modeling System*, HyperCube, Inc.: Waterloo, Oterio, Canada; **2002**.